Electronic supporting information for

Value-added methanol electroreforming coupled with green hydrogen production at the edge interface of 2D boron nanosheets

Arunprasath Sathyaseelan[1], Karthikeyan Krishnamoorthy[1,2,3], Parthiban Pazhamalai[1,2], Noor Ul Haq Liyakath Ali[1] and Sang-Jae Kim[1,2,4]*

[1]Nanomaterials & System Laboratory, Major of Mechatronics Engineering, Faculty of Applied Energy System, Jeju National University, Jeju, 63243, South Korea

[2]Research Institute of New Energy Industry (RINEI), Jeju National University, Jeju, 63243, South Korea

[3]Department of Physics, School of Advanced Sciences, Vellore Institute of Technology, Vellore, 632014, India

[4]Nanomaterials & System Lab, Major of Mechanical System Engineering, College of Engineering, Jeju National University, Jeju, 63243, South Korea

[*]Corresponding author Email: kimsangj@jejunu.ac.kr

1. Experimental Section:

The faradaic efficiency of the hybrid water electrolyser device was calculated by water drainage method using lab made H-type membrane water electrolyser device.

The amount of hydrogen gas (H_2) evolved during the electrolysis process was collected through measuring cylinder by applying a constant current density with various time interval. The amount of hydrogen released as theoretical were calculated using following faraday's law.

$V_{Theo}=IRTt/PzF$ …….(1)

V_{Theo} = Theoretical volume of evolved gas

I= working current density (mA cm^{-2})

T is working temperature (K) and 't' is time interval (s)

R is the gas constant and 'P' is the working pressure

F is the Faraday's constant (F=96485 C)

z is the number of electrons for generating 1 mol H_2 (z=2)

Faradaic efficiency (ηF) was determined by ratio of measured gas volume (V_{meas}) and theoretically calculated volumes (V_{Theo}) as given in equation

$\eta F=V_{meas}/V_{Theo}$ …….(2)

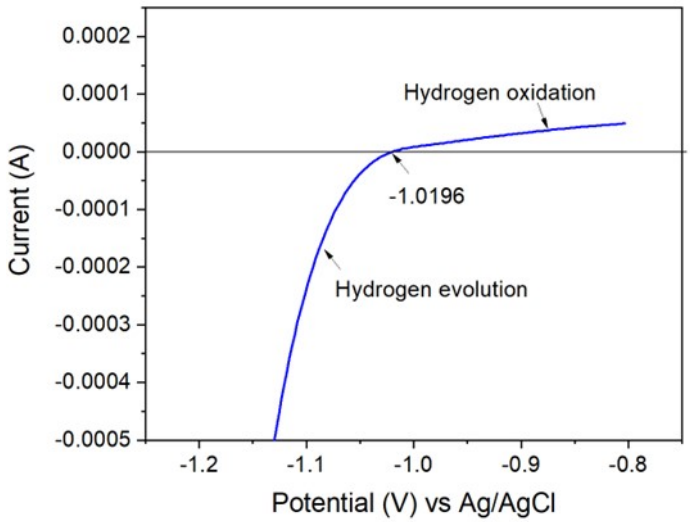

Figure S1: Calibration of Ag/AgCl in H_2 saturated 1.0 M KOH electrolyte.

The calibration of Ag/AgCl reference electrode was done in a H_2 saturated 1.0 M KOH electrolyte at a scan rate of 1 mV/s. From the LSV, the current which crosses zero was identifies as a thermodynamic potential of hydrogen electrode and the potential was found to be 1.0196 V. In 1 M KOH, $E_{RHE} = E_{Ag/AgCl} + 1.0196$ V. [1–3]

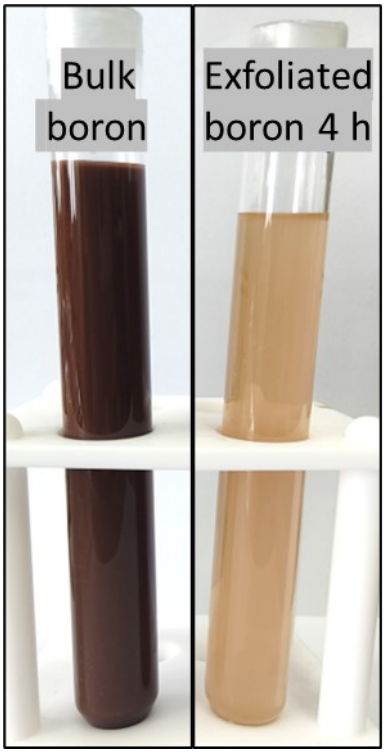

Figure S2: Digital photograph of bulk boron and exfoliated boron nanosheets 4 h.

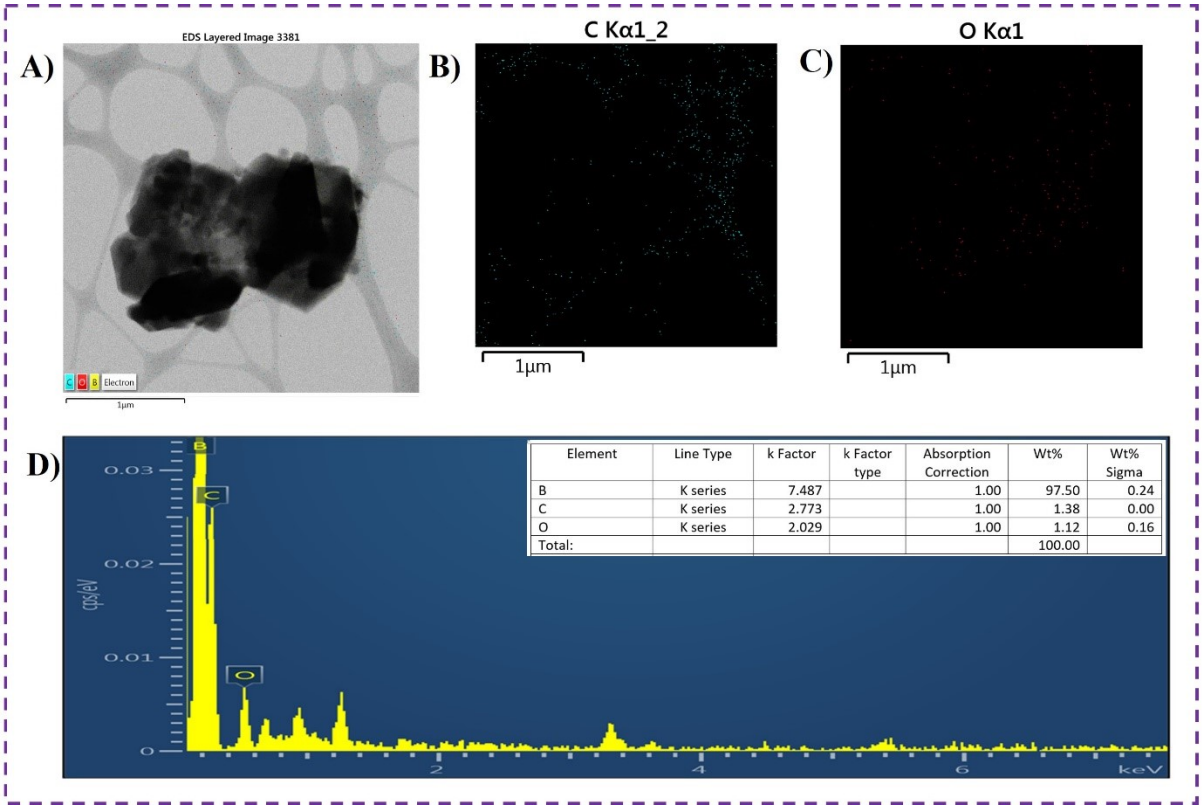

Element	Line Type	k Factor	k Factor type	Absorption Correction	Wt%	Wt% Sigma
B	K series	7.487		1.00	97.50	0.24
C	K series	2.773		1.00	1.38	0.00
O	K series	2.029		1.00	1.12	0.16
Total:					100.00	

Figure S3: HR-TEM images of bulk boron. (A) Overlay mapping, (B-D) elemental mapping analysis of C and O. (E) Corresponding EDS spectrum.

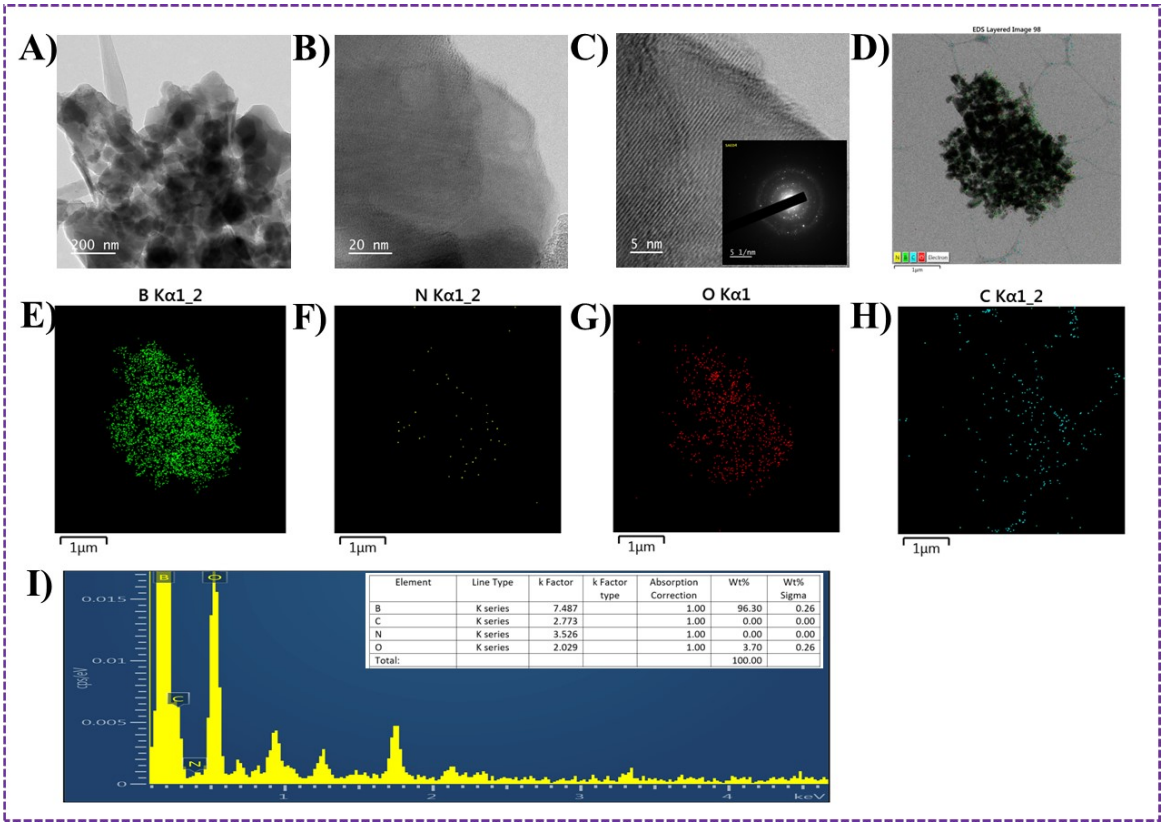

Figure S4. Morphological analysis of eBNS-2. (A-C) HR-TEM images of eBNS-2 at different magnifications and inset in (C) present the corresponding SAED pattern. (D) EDS overlay mapping and (E-H) individual elemental mapping of B, N, O, C. (I) EDS spectrum of eBNS-2.

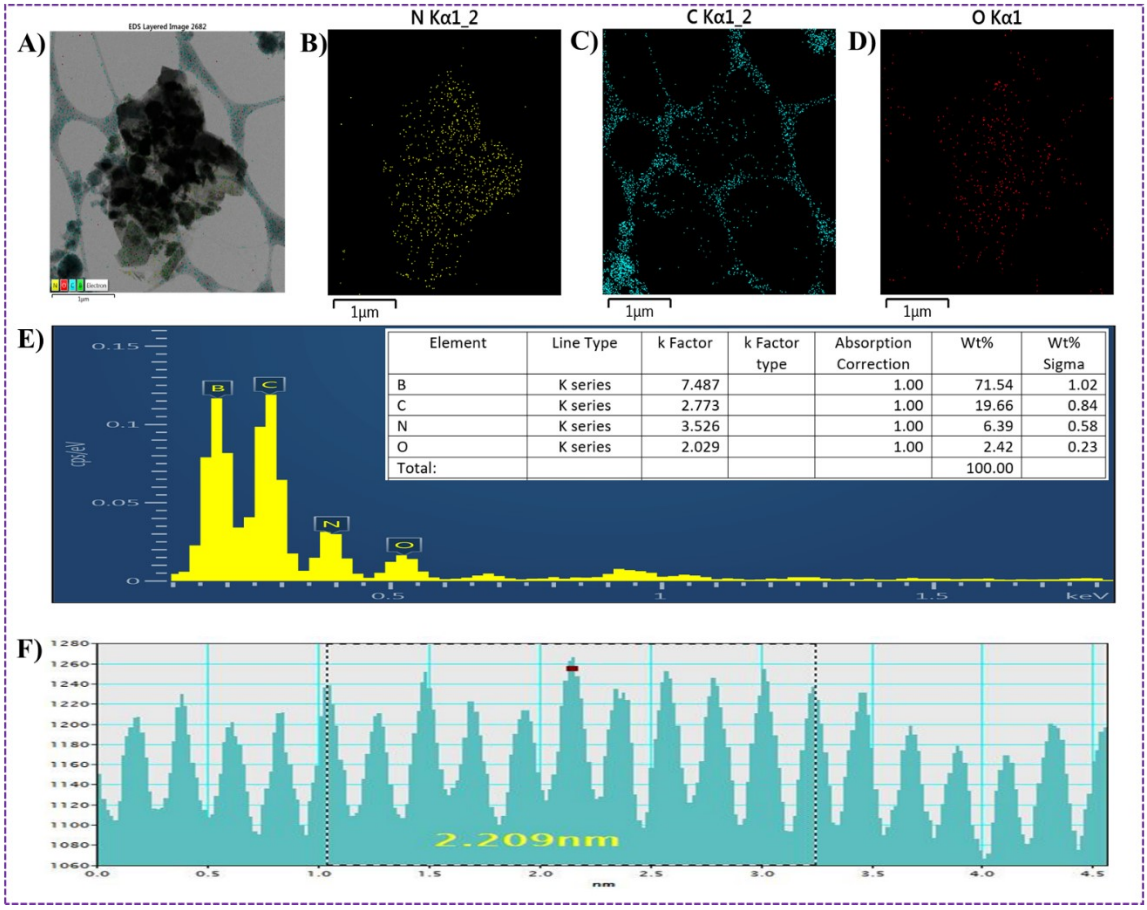

Element	Line Type	k Factor	k Factor type	Absorption Correction	Wt%	Wt% Sigma
B	K series	7.487		1.00	71.54	1.02
C	K series	2.773		1.00	19.66	0.84
N	K series	3.526		1.00	6.39	0.58
O	K series	2.029		1.00	2.42	0.23
Total:					100.00	

Figure S5: HR-TEM images of exfoliated boron nanosheets. (A) Overlay mapping, (B-D) elemental mapping analysis of N, C and O. (E) Corresponding EDS spectrum. (F) average d-spacing distribution profile of eBNS-4.

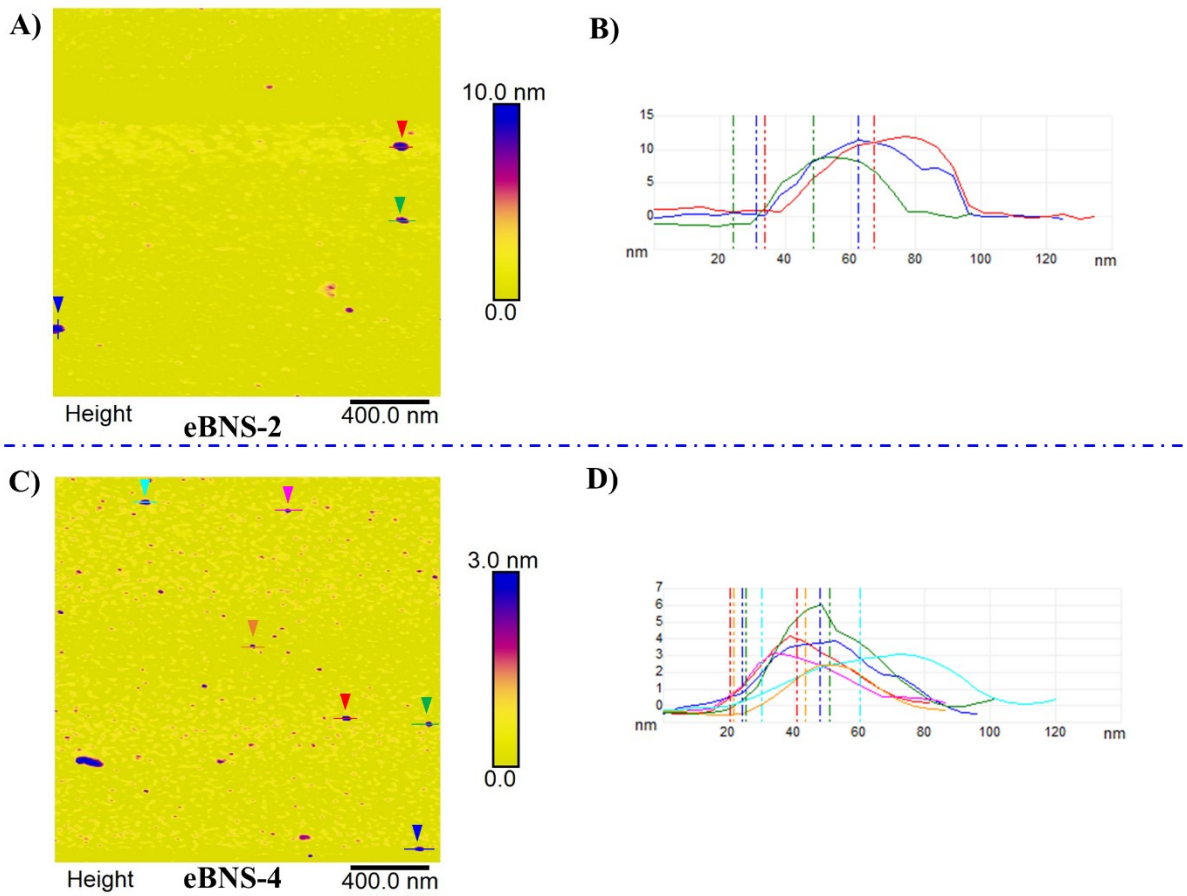

Figure S6. (A-D) AFM analysis of eBNS-2 and eBNS-4 with section analysis at different places.

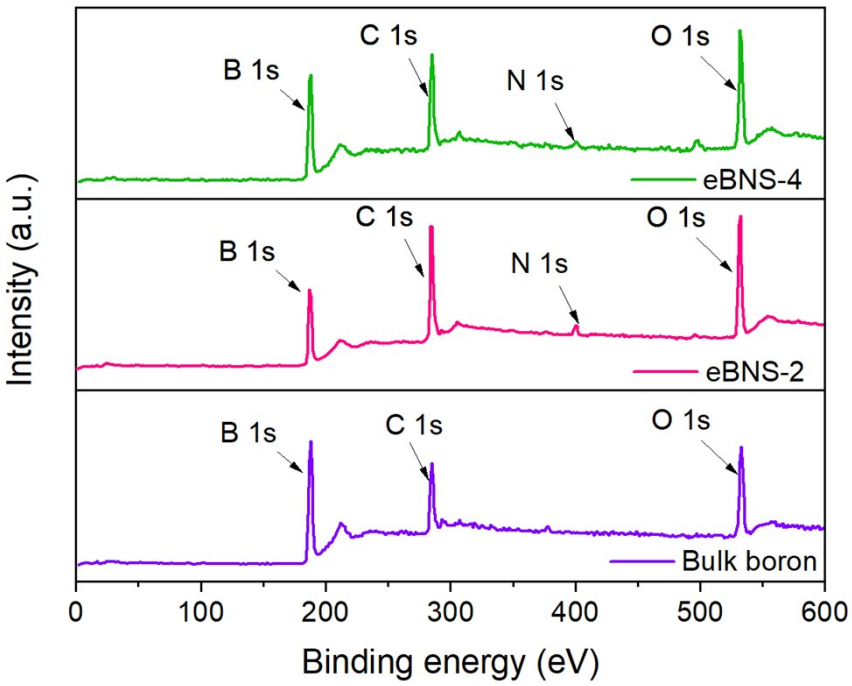

Figure S7. X-ray photoelectron survey spectra of eBNS-4 eBNS-2 and BB.

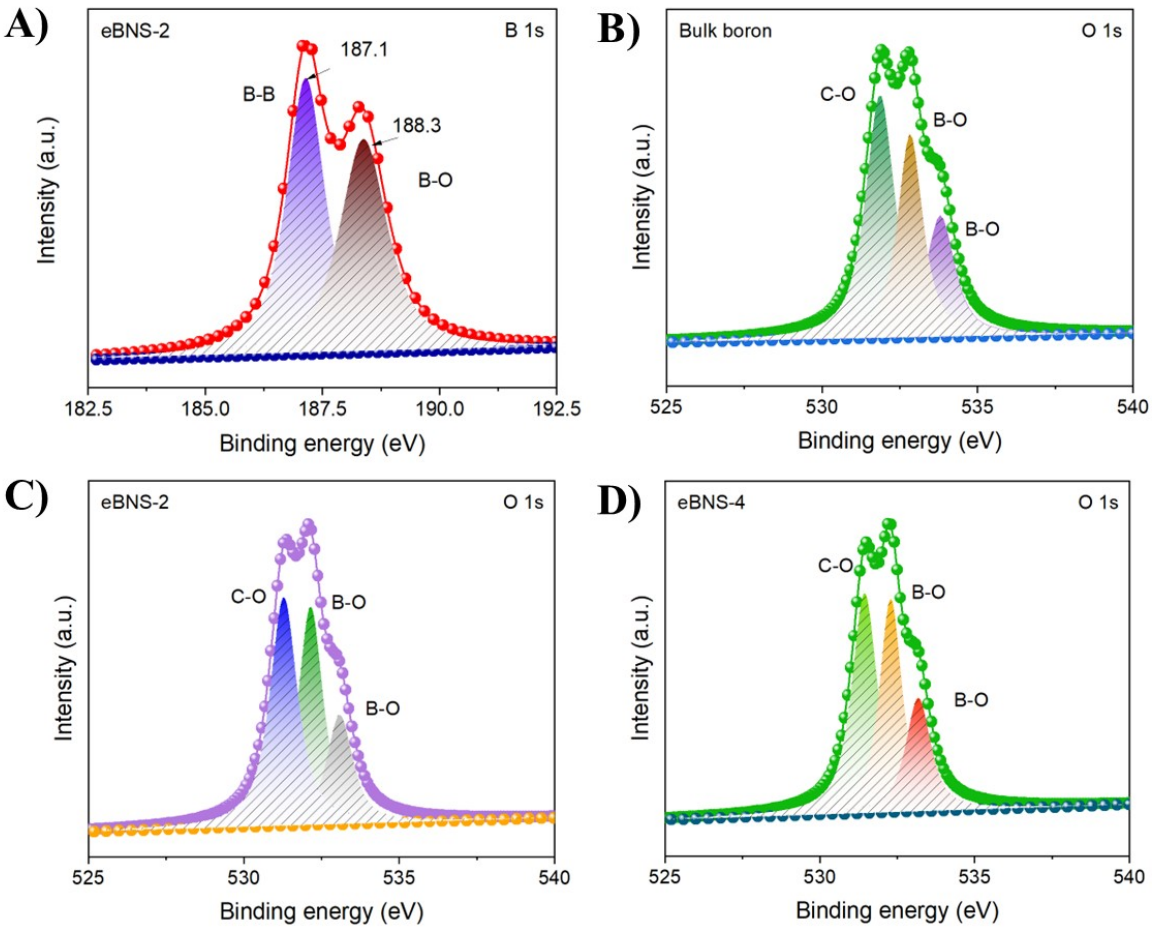

Figure S8. (A) Deconvoluted B1s spectrum of eBNS-2, (B-D) O 1s core-level spectrum presented in the bulk boron, eBNS-2, and eBNS-4.

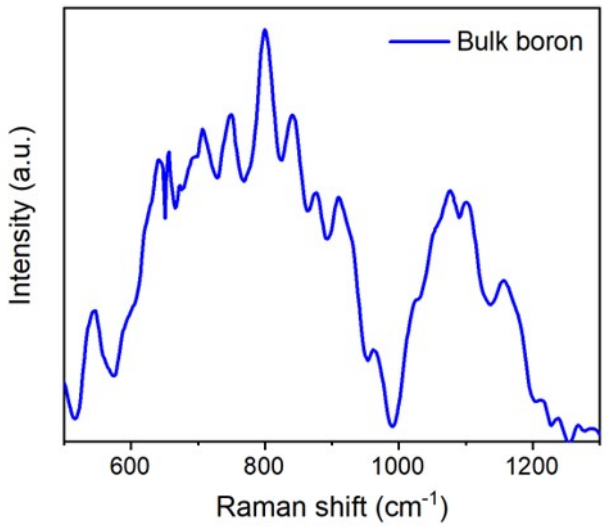

Figure S9. Laser Raman spectra of bulk boron.

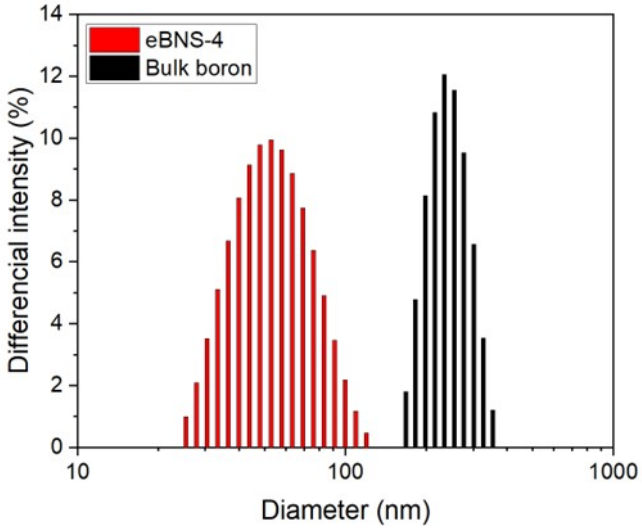

Figure S10. Particle size distribution analysis of eBNS-4 and BB.

Mechanism of hydrogen evolution reaction and oxygen evolution reaction occurring at the surface the few layered boron and bulk boron electrodes in the alkaline medium are given below:

Mechanism of hydrogen evolution reaction occurring at the surface of prepared catalysts are given below.

$H_2O + e^- + * \rightarrow H* + HO^-$ *(1)*

Volmer (120 mV dec^{-1})

$H_2O + e^- + H* \rightarrow H_2 + HO^-$ *(2)*

Heyrovsky (40 mV dec^{-1})

$H* + H* \rightarrow H_2$ *(3)*

Tafel (30 mV dec^{-1})

Mechanism of oxygen evolution reaction occurring at the surface prepared catalysts are given below.

$$* + OH^- \rightarrow *OH^- + e^- \quad (4)$$

(Tafel slope: 120 mV dec^{-1})

$$*{-}OH + OH \rightarrow *{-}O^- + H_2O \quad (5)$$

(Tafel slope: 60 mV dec^{-1})

$$*{-}O^- \rightarrow *{-}O + e^- \quad (6)$$

(Tafel slope: 40 mV dec^{-1})

$$2*{-}O \rightarrow 2* + O_2\uparrow \quad (7)$$

(Tafel slope: 15 mV dec^{-1})

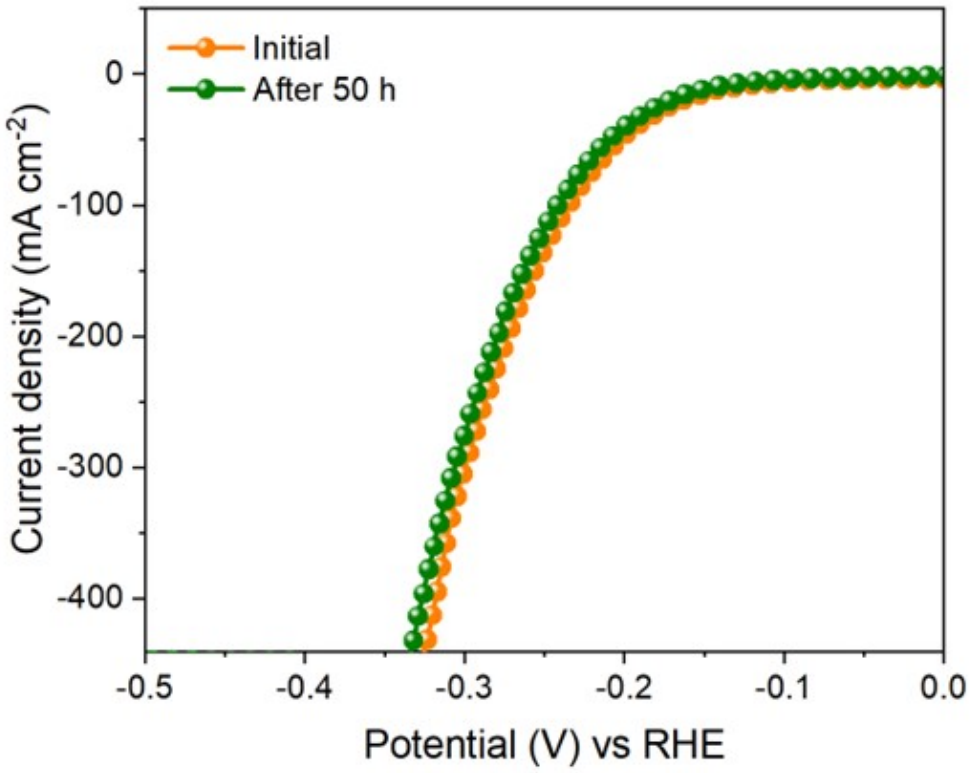

Figure S11. HER LSV polarization before and after the stability test.

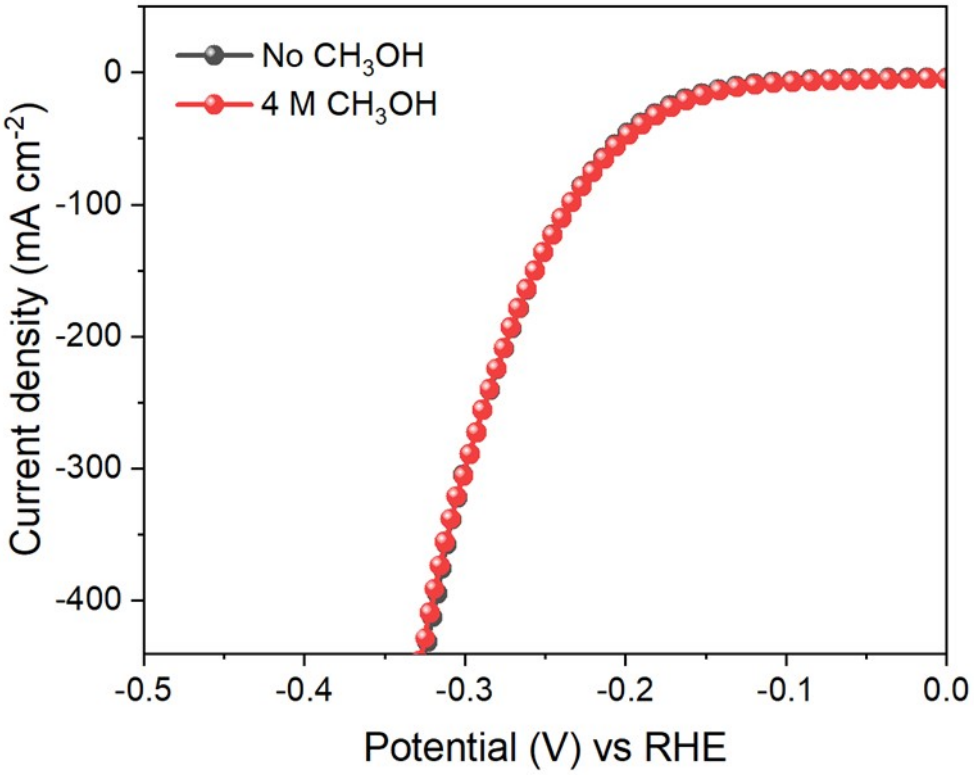

Figure S12. HER LSV polarization of eBNS/NF-4 measured in 1.0 M KOH with 4 M CH_3OH.

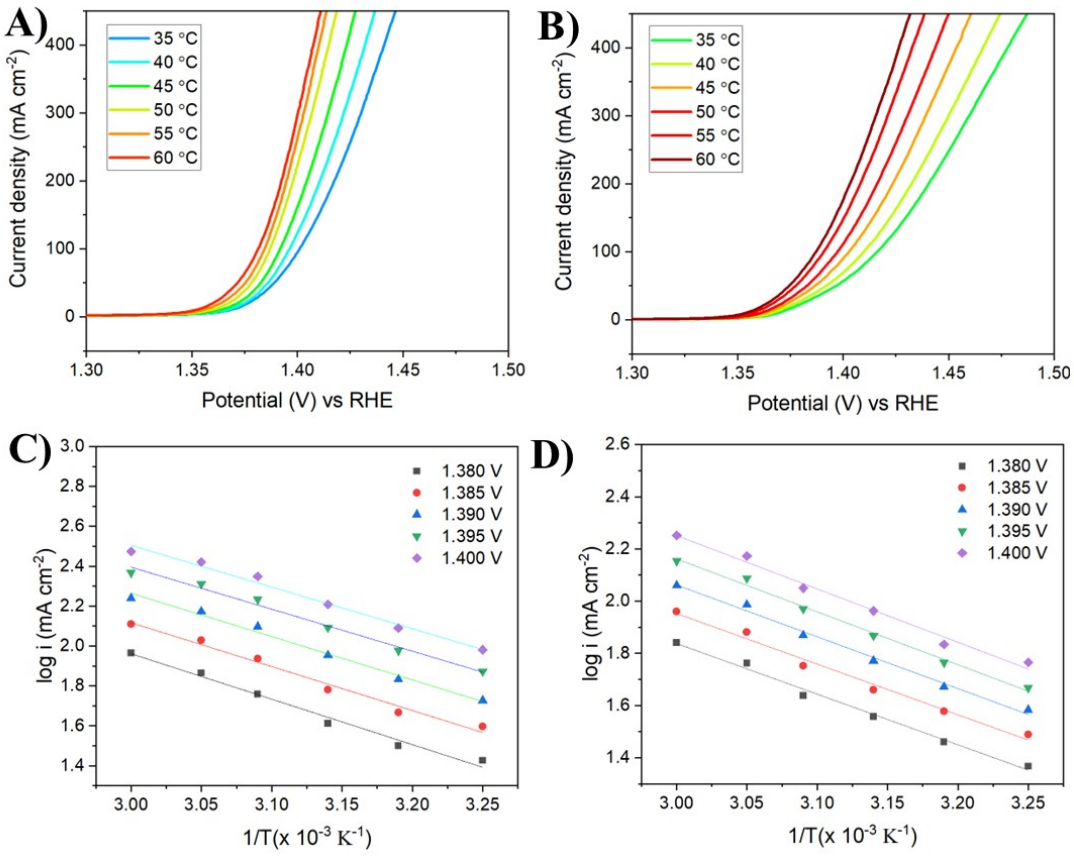

Figure S13. Temperature dependent MOR analysis of (A) eBNS/NF-4 and (B) BB/NF. Arrhenius plot of MOR logarithmic current densities at various measured potentials for (C) eBNS/NF-4 and (D) BB/NF.

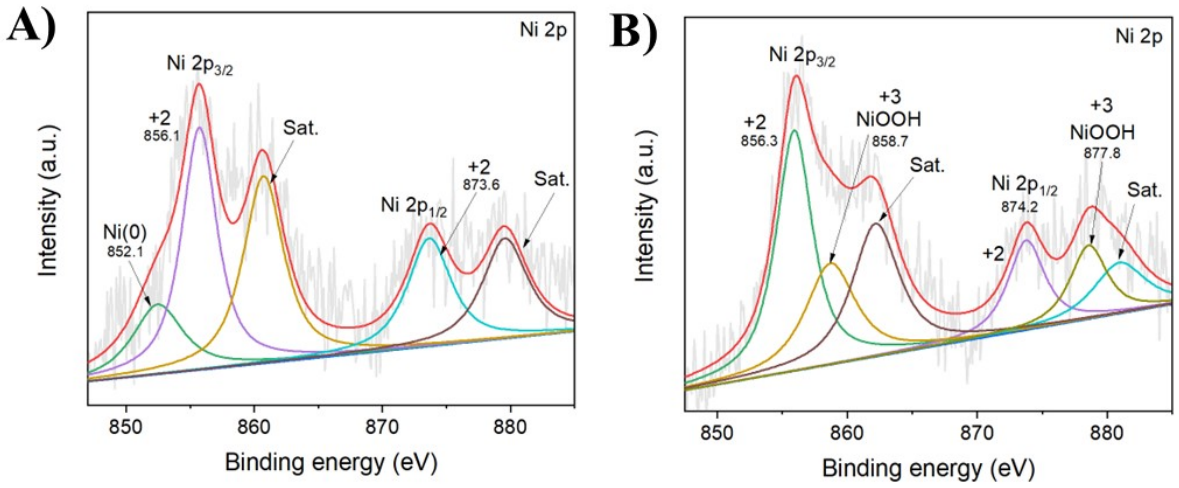

Figure S14. Deconvoluted XPS Ni 2p core level spectrum of eBNS/NF-4 before (A) and after stability test (B)

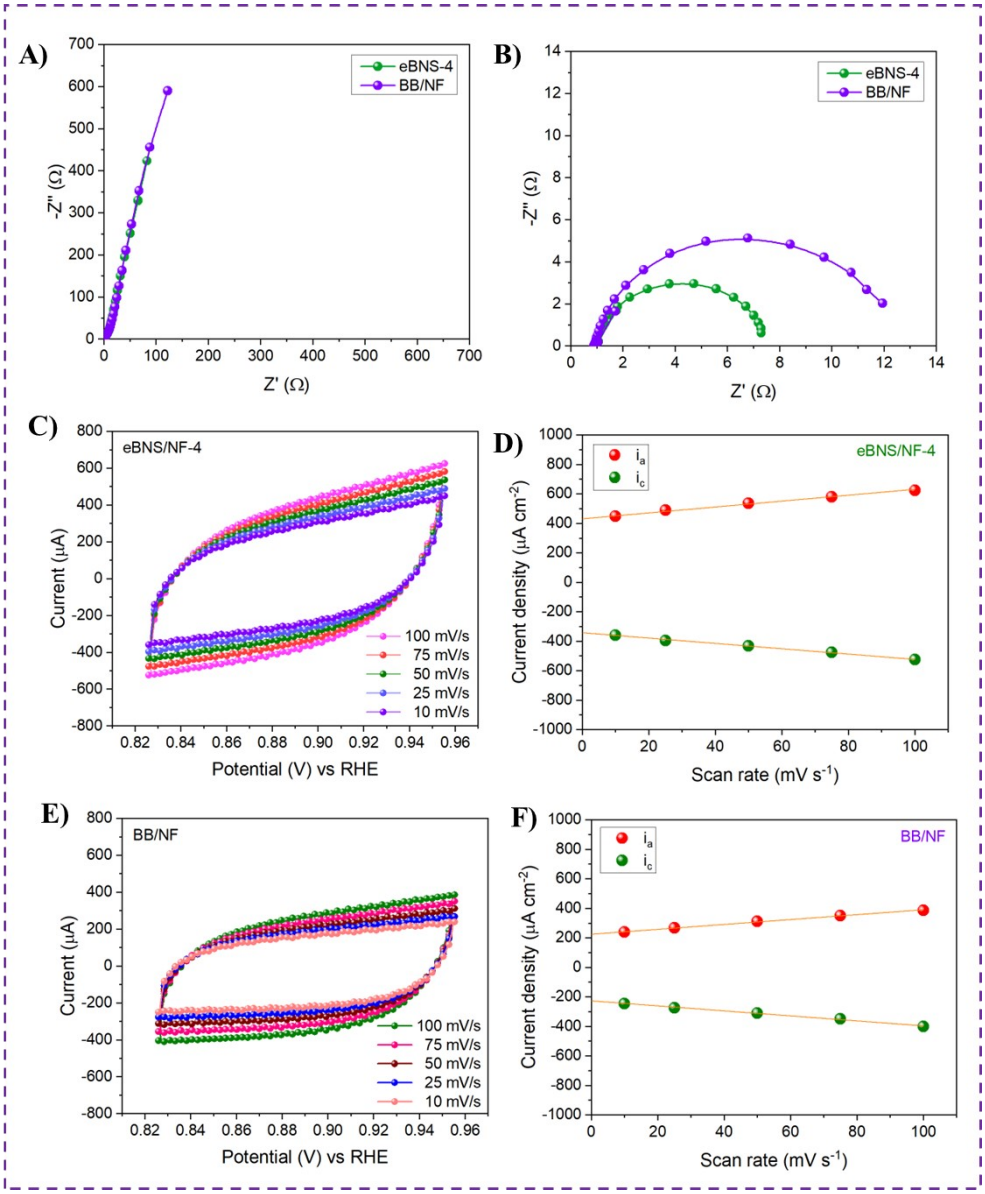

Figure S15: Electrode kinetics of eBNS/NF-4 and BB/NF. (A) EIS spectrum of eBNS/NF-4 and BB/NF electrodes measured at a frequency range of 10000 Hz to 0.1 Hz in 1.0 M KOH at OCP. (B) Nyquist plot at an applied potential of 1.5 V vs. RHE. (C and E) CV profiles of an eBNS/NF-4 and BB/NF. (D and F) Corresponding capacitive currents rates with a scan rate of 10, 25, 50, 75 and 100 mV s^{-1} in 1.0 M KOH.

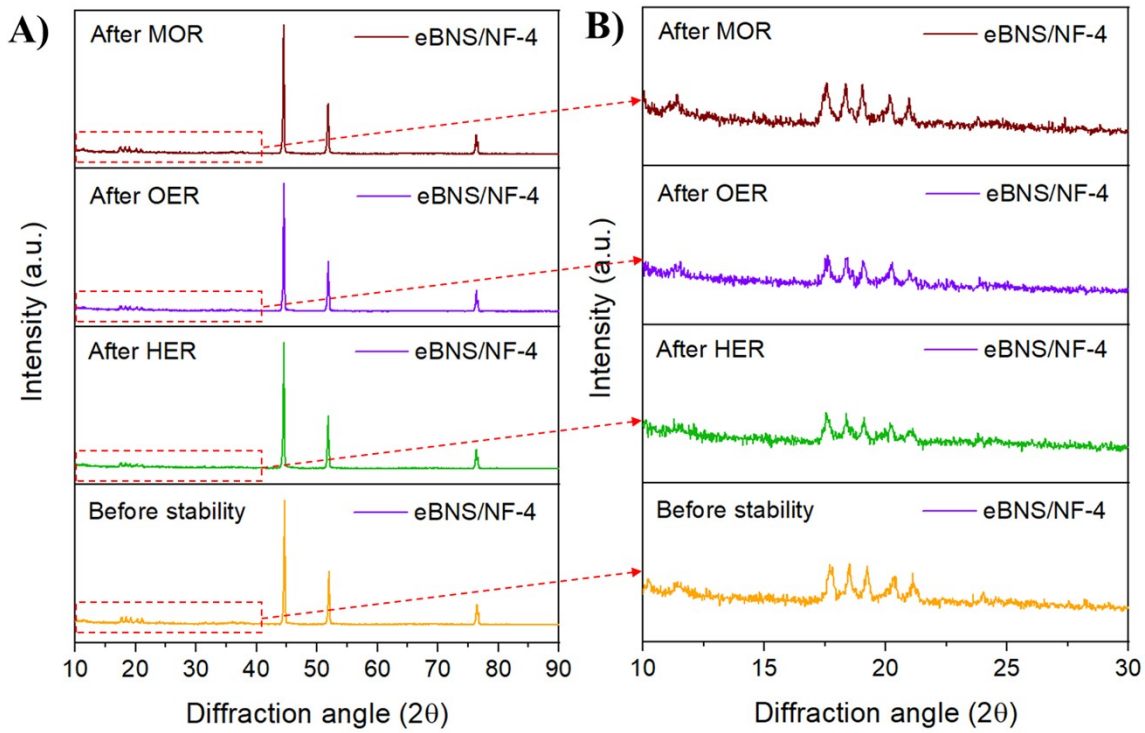

Figure S16. XRD analysis of eBNS-4 electrode fabricated on Nickel foam. (A) Comparative XRD pattern of as prepared electrode and after electrochemical reaction (HER, OER and MOR) (B) Zoomed version of the Figure A confirms the major peaks preserved after the stability test.

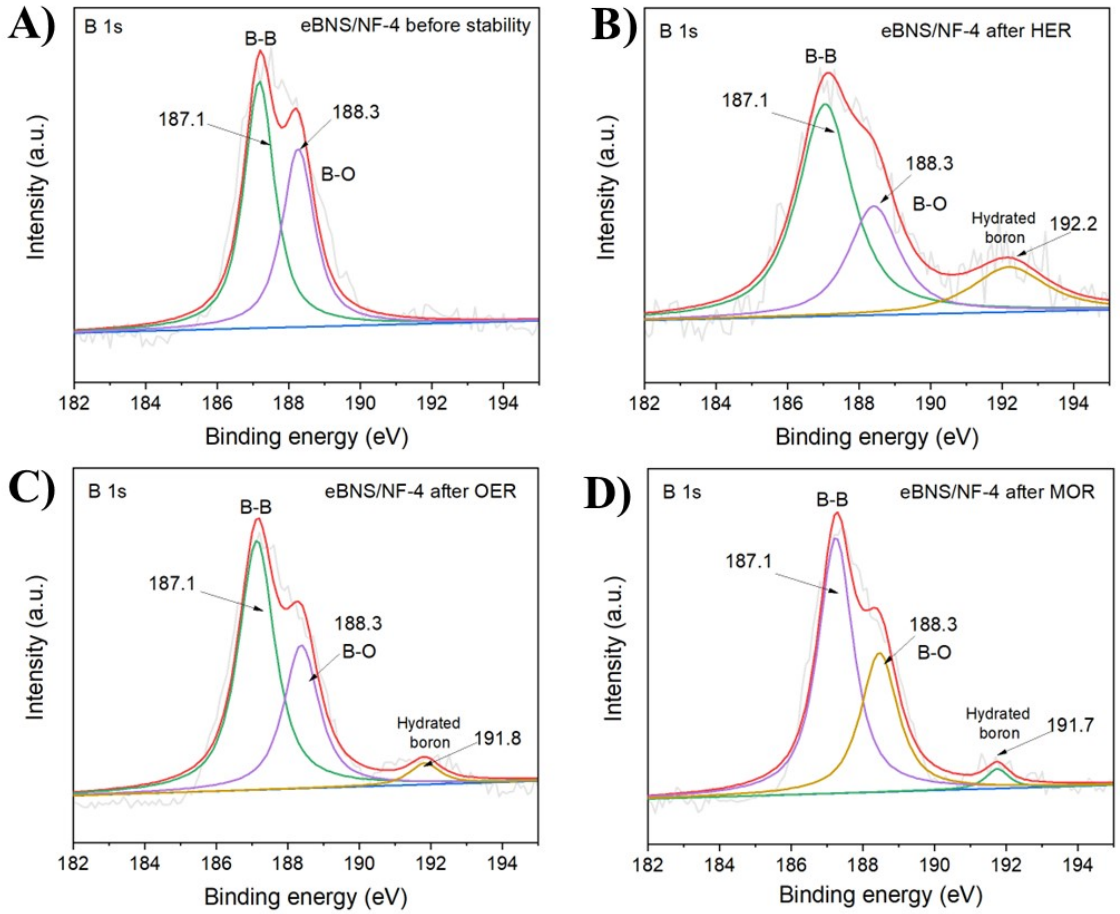

Figure S17. XPS analysis of eBNS/NF-4 before and after stability test. (A) B 1s spectrum before and after stability and (B-D) B 1s core-level spectrum after HER, OER and MOR.

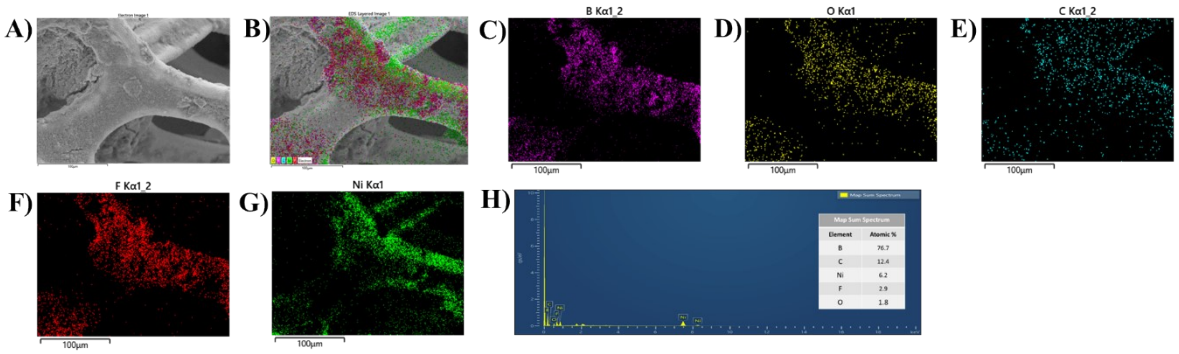

Figure S18. Morphological and elemental analysis of eBNS-4 electrode fabricated on Nickel foam. (A) FE-SEM micrographs of eBNS/NF-4 recorded under 100 µm magnification. (B) Overlay map, (C-G) Elemental maps of (C) boron, (D) oxygen, (E) carbon, (F) fluorine, (G) nickel. (H) Presents the EDX spectrum of the eBNS/NF-4 electrode.

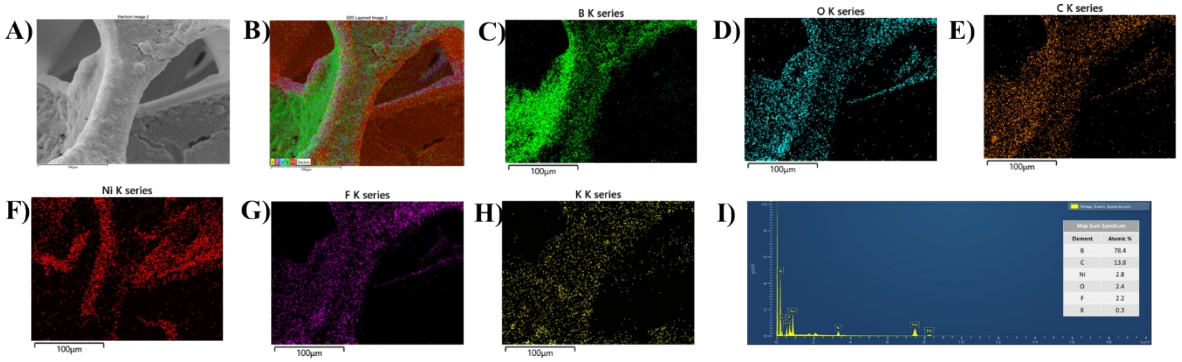

Figure S19. Morphological and elemental analysis of eBNS-4 electrode fabricated on Nickel foam after the HER stability test. (A) FE-SEM micrographs of eBNS/NF-4 recorded under 100 µm magnification. (B) Overlay map, (C-H) Elemental maps of (C) boron, (D) oxygen, (E) carbon, (F) nickel, (G) fluorine and (H) potassium. (I) Presents the EDX spectrum of the eBNS/NF-4 electrode.

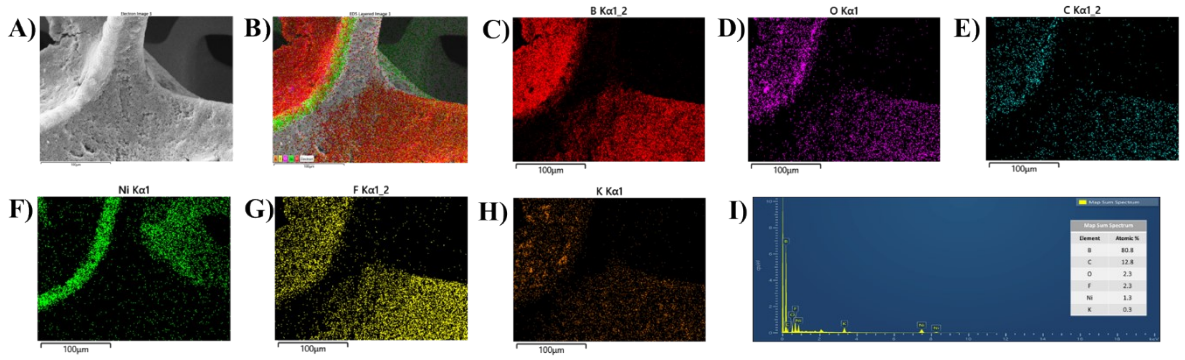

Figure S20. Morphological and elemental analysis of eBNS-4 electrode fabricated on Nickel foam after the OER stability test. (A) FE-SEM micrographs of eBNS/NF-4 recorded under 100 µm magnification. (B) Overlay map, (C-H) Elemental maps of (C) boron, (D) oxygen, (E)

carbon, (F) nickel, (G) fluorine and (H) potassium. (I) Presents the EDX spectrum of the eBNS/NF-4 electrode.

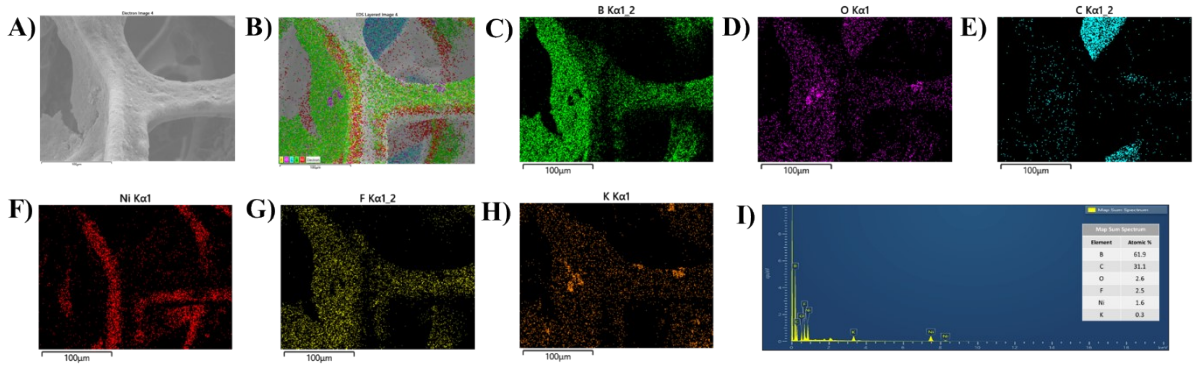

Figure S21. Morphological and elemental analysis of eBNS-4 electrode fabricated on Nickel foam after the MOR stability test. (A) FE-SEM micrographs of eBNS/NF-4 recorded under 100 µm magnification. (B) Overlay map, (C-H) Elemental maps of (C) boron, (D) oxygen, (E)

carbon, (F) nickel, (G) fluorine and (H) potassium. (I) Presents the EDX spectrum of the eBNS/NF-4 electrode.

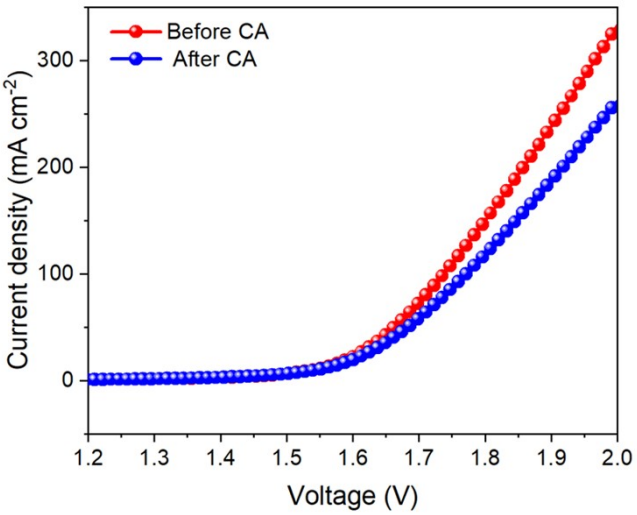

Figure S22. LSV polarization of hybrid electrolyser before and after durability test.

Table S1. Over all comparison analysis of eBNS/NF-4 with the recently reported catalysts

Electrocatalysts	Analysis	Overpotential (η) (mV cm^{-2})	Tafel slope (mV dec^{-1})	Electrolyte	Ref.
eBNS/NF-4	HER	146	68	1 M KOH and 1 M CH_3OH	This work
	OER	291	40		
	MOR	190	52		
	Water splitting	1.71 V	-		
	Hybrid water splitting	1.57 V	-		
CoP_x@NC	HER	187	58.5	1 M KOH	[4]
	OER	380	68.1		
	Water splitting	1.71 V	-		
Co/CoP–HNC	HER	180	105.6	1 M KOH	[5]
	OER	300	44.2		
	Water splitting	1.68 V	-		
Mo-CoP	HER	118	69	1 M KOH	[6]
	OER	317	82		
	Water splitting	1.7 V	-		

h-CoP@NC	HER	196	84.5	1 M KOH	[7]
	OER	339	95.1		
	Water splitting	1.764 V	-		
$Co_2P/Mo_2C/Mo_3Co_3C$@C	HER	182	65	1 M KOH	[8]
	OER	362	82		
	Water splitting	1.74 V	-		
NC/Co/CoP/CP	HER	208	126	1 M KOH	[9]
	OER	350	133		
	Water splitting	1.72 V	10		
$Co/CeO_2/Co_2P$/CoP@NC	HER	195	66	1 M KOH	[10]
	OER	307	99.6		
	Water splitting	1.76 V	-		
CoP@NC/NCNT	HER	177	79	1 M KOH	[11]
	OER	324	52		
	Water splitting	1.72 V	-		
CoP@FeCoP/NC YSMPs	HER	141	56.34	1 M KOH	[12]
	OER	238	47.98		
	Water splitting	1.68 V	-		

Table S2. Mass activity of eBNS/NF-4 and BB/NF for HER.

Overpotential (mV)	**Mass activity (HER) (A/g)**	
	Bulk boron	**Few layered boron**
@150	-0.8	-2.474
@200	-0.922	-11.622
@250	-1.902	-29.09
@300	-8.6	-57.824

Calculation for Active sites confirmation

Total no of B (active sites) = 1.1141×10^{23}

Turn over frequency calculation

TOF = Current density × Electrode area × 6.023×10^{23}(H_2/s)/2(n) × F(faraday constant) × Active sites

n = 2 for HER and 4 for OER.

Table S3. TOF calculated for the prepared catalysts for HER

Overpotential (mV)	TOF (HER) (H_2/s)	
	Bulk boron	**Few layered boron**
@150	$1.12E^{-4}$	$3.46E^{-4}$
@200	$1.29E^{-4}$	0.0016
@250	$2E^{-4}$	0.004
@300	0.0012	0.008

Table S4. Mass Activity of eBNS/NF-4 and BB/NF for OER.

Overpotential (mV)	Mass activity (A/g)	
	Bulk boron	**Few layered boron**
@300	0.464	2.946
@350	0.918	16.302
@400	2.644	41.4
@450	7.282	73.266

Table S5. TOF calculated for the prepared catalysts for OER

Overpotential (mV)	TOF (O_2/s)	
	Bulk boron	**Few layered boron**
@300	$3E^{-5}$	$2E^{-4}$
@350	$6E^{-5}$	$1E^{-3}$
@400	$1E^{-4}$	0.002
@450	$5E^{-4}$	0.005

Table S6. Hybrid water electrolyser performance of eBNS/NF-4‖eBNS/NF-4 device with the recently reported hybrid devices

Electrocatalysts	Analysis	Electrolyte	Cell voltage at 10 mA cm^{-2}	Ref.
$Ni(OH)_2$/NF	Hybrid water splitting	1 M KOH + 0.5 M CH_3OH	1.52 V	13
$CoS_x(OH)_y$/CP	Hybrid water splitting	1 M KOH + 3 M CH_3OH	1.578 V	14
$Ni_{0.33}Co_{0.67}(OH)_2$/NF	Hybrid water splitting	1 M KOH + 0.5 M CH_3OH	1.50 V	15
NC@$CuCo_2N_x$/CF	Hybrid water splitting	1 M KOH + 0.015 M benzyl alcohol	1.55 V	16
Ni_2P/NF	Hybrid water splitting	1 M KOH + 0.01 M HMF	1.65 V	17

Co-S-P/CC	Hybrid water splitting	1 M KOH + 1 M C_2H_5OH	1.63	[18]
α-$Co(OH)_2$/CP	Hybrid water splitting	1 M KOH + 3 M CH_3OH	1.758 V	[14]
eBNS/NF-4	Hybrid water splitting	1 M KOH + 4 M CH_3OH	1.55 V	This work

References

1 Y. Zhu, W. Zhou, Y. Zhong, Y. Bu, X. Chen, Q. Zhong, M. Liu and Z. Shao, *Adv. Energy Mater.*, 2017, **7**, 1602122.

2 S. Wang, J. Nai, S. Yang and L. Guo, *ChemNanoMat*, 2015, **1**, 324–330.

3 S. Li, S. Sirisomboonchai, X. An, X. Ma, P. Li, L. Ling, X. Hao, A. Abudula and G. Guan, *Nanoscale*, 2020, **12**, 6810–6820.

4 J.-S. Li, L.-X. Kong, Z. Wu, S. Zhang, X.-Y. Yang, J.-Q. Sha and G.-D. Liu, *Carbon N. Y.*, 2019, **145**, 694–700.

5 Y. Hao, Y. Xu, W. Liu and X. Sun, *Mater. Horizons*, 2018, **5**, 108–115.

6 L. Li, Y. Guo, X. Wang, X. Liu and Y. Lu, *Langmuir*, 2021, **37**, 5986–5992.

7 X.-Z. Song, Y.-H. Zhao, W.-B. Yang, Y.-L. Meng, X. Chen, Z.-Y. Niu, X.-F. Wang and Z. Tan, *ACS Appl. Nano Mater.*, 2021, **4**, 13450–13458.

8 X. Li, X. Wang, J. Zhou, L. Han, C. Sun, Q. Wang and Z. Su, *J. Mater. Chem. A*, 2018, **6**, 5789–5796.

9 M. Cong, D. Sun, L. Zhang and X. Ding, *Chinese J. Catal.*, 2020, **41**, 242–248.

10 X.-Z. Song, Q.-F. Su, S.-J. Li, G.-C. Liu, N. Zhang, W.-Y. Zhu, Z.-H. Wang and Z. Tan, *Int. J. Hydrogen Energy*, 2020, **45**, 30559–30570.

11 Z. Wu, B. Liu, H. Jing, H. Gao, B. He, X. Xia, W. Lei and Q. Hao, *J. Colloid Interface Sci.*, 2023, **629**, 22–32.

12 J. Shi, F. Qiu, W. Yuan, M. Guo and Z.-H. Lu, *Chem. Eng. J.*, 2021, **403**, 126312.

13 J. Hao, J. Liu, D. Wu, M. Chen, Y. Liang, Q. Wang, L. Wang, X.-Z. Fu and J.-L. Luo, *Appl. Catal. B Environ.*, 2021, **281**, 119510.

14 K. Xiang, D. Wu, X. Deng, M. Li, S. Chen, P. Hao, X. Guo, J. Luo and X. Fu, *Adv. Funct. Mater.*, 2020, **30**, 1909610.

15 M. Li, X. Deng, K. Xiang, Y. Liang, B. Zhao, J. Hao, J. Luo and X. Fu, *ChemSusChem*, 2020, **13**, 914–921.

16 J. Zheng, X. Chen, X. Zhong, S. Li, T. Liu, G. Zhuang, X. Li, S. Deng, D. Mei and J.-G. Wang, *Adv. Funct. Mater.*, 2017, **27**, 1704169.

17 B. You, N. Jiang, X. Liu and Y. Sun, *Angew. Chemie Int. Ed.*, 2016, **55**, 9913–9917.

18 S. Sheng, K. Ye, L. Sha, K. Zhu, Y. Gao, J. Yan, G. Wang and D. Cao, *Inorg. Chem. Front.*, 2020, **7**, 4498–4506.